Phys. Status Solidi C **6**, No. 9, 2056–2059 (2009) / **DOI** 10.1002/pssc.200881757

physica status solidi c
www.pss-c.com
current topics in solid state physics

Light polarized resonant Raman spectra from individual single- and double-wall carbon nanotubes

J. Judek[1], D. Brunel[2], T. Mélin[2], M. Marczak[1], M. Zdrojek[1], W. Gebicki[1], and L. Adamowicz[*,1]

[1] Faculty of Physics, Warsaw University of Technology, Koszykowa 75, 00-662 Warsaw, Poland
[2] Institut d'Electronique, de Microélectronique et de Nanotechnologie, CNRS UMR 8520, Dpt ISEN, Avenue Poincaré, 59652 Villeneuve d'Ascq, France

Received 17 September 2008, accepted 9 January 2009
Published online 14 July 2009

PACS 63.22.Gh, 71.15.Mb, 78.30.Na, 78.67.Ch

[*] Corresponding author: e-mail adamo@if.pw.edu.pl

Measured light polarization dependent resonant Raman spectra from spatially isolated semiconducting single- and double-wall carbon nanotubes are reported. Most of the observed modes intensities exhibit two or fourfold symmetry, for VV and VH configuration, respectively. Weak quantitative changes in the G bands have been observed suggesting different subbands transitions $E^{v}_{\mu} \rightarrow E^{c}_{\mu}$ contribution. Model explaining both the angular variation and week quantitative changes is presented. Selected carbon nanotubes electronic and optical properties are studied using the *ab initio* calculations in order to complete the outlook.

1 Introduction The presence of one-dimensional van Hove singularities (vHS) in the nanotubes' electronic DOS is responsible for strong optical response of carbon nanotubes, thus, making possible measurement of Raman signals even from individual carbon nanotube. Many features have been studied. The most significant of them are: the radial breathing mode (RBM) – in the context of strong frequency dependence on tube diameter, the tangential modes or G band – providing symmetry-related information and the defect-induced double-resonant D band.

The first polarization dependent Raman spectra of spatially separated thin ropes composed of individual SWNTs were performed by Duesberg *et al*. [1]. The orientation dependence of the intensity of investigated there Raman modes showed two-fold symmetry. The measured angular dependences [1] do not follow theoretical predictions [2, 3] obtained under nonresonant conditions. The maximum signal is always observed when the polarization of the incident light is parallel to the nanotube axis. This behaviour [1] was ascribed to structurally anisotropic depolarization and resonance effects which cause a breakdown of selection rules.

A similar polarization effect was observed for aligned and bundled multi-wall carbon nanotubes (MWNT) [3]. Theoretically previewed [2, 3] characteristic minimum of G-band A (A_{1g}) mode intensity at $\varphi \sim 55^{o}$ for SWNT has been confirmed experimentally also in the case of aligned MWNT [4] in VV configuration (meaning parallel polarization geometry of incident and scattered light). Polarized Raman studies of aligned bundle of semiconducting SWNTs have allowed identifying the symmetry and the dependence on nanotube geometry of the G-band modes [5]. The relative Raman intensities of G-band modes belonging to different irreducible representations can be basically explained by symmetry considerations. The observed discrepancies [5] are attributed to the presence of different chiral tubes in the bundle.

Further polarized Raman studies of isolated SWNT have shown that it acts as a dipolar antenna polarized along the tube axis (Z) [6]. Emission of Raman scattered light is strongly suppressed when the incident or scattered light is polarized perpendicular (X) to the nanotube axis (Z), in agreement with previous results [1]. However, the neighbouring isolated SWNTs can modify this antenna behaviour. The antenna effect [6] is strongly operative for

large diameter SWNT resonant with various transitions, for either the incident or scattered photons. For light polarized along the tube axis (Z) the strong resonance effect breaks the symmetry selection rules and one can observe symmetry forbidden modes. Experimentally observed G-band modes can be identified by polarization selection rules, when the light is not polarized parallel to the tube axis (Z), in good agreement with the theoretical predictions [2, 3].

More recent results [7, 8] have shown the importance of the resonance with light polarized perpendicular (X) to SWNT axis. Assuming that the first-order Raman signal from isolated SWNT can be seen in the resonance with vHS one can apply the four possible Raman processes involving electron – incident photon, electron – phonon and electron – scattered photon interactions, as described in [2, 7–9]. In particular, the phonon modes belonging to the E_2 symmetry representation can be observed only for (XX) scattering geometry (see Fig. 1) with $E^v_\mu \rightarrow E^c_{\mu\pm1}$ vHSs transitions. Here, E^v_μ and $E^c_{\mu'}$ (with $\mu' = \mu$ or $\mu \pm 1$ for Z and X polarization, respectively) label irreducible representations of the CNT symmetry group to which belong wave functions from the valence and conduction band, respectively, involved in the electronic transitions. It is interesting to note, that relatively high intensity (XX) spectrum has been observed indicating resonance with $E^v_\mu \rightarrow E^c_{\mu\pm1}$ electronic transition. In contrast to the previous results no substantial reduction of the scattered light has been observed. The disagreement with the expected depolarization effect is explained as a characteristic resonance feature. The antenna behaviour seems to be an effect that appears for the exciting laser light in the resonance with vHS electronic transitions $E^v_\mu \rightarrow E^c_\mu$; hence, the light scattering on A symmetry allowed phonon modes is most effective for the Z polarization.

To our knowledge polarized Raman spectra from individual double-wall nanotube (DWNT) have not yet been studied. In this paper we present the polarized Raman spectra from individual DWNT as well as for the individual SWNT, in the conditions of complete spatial isolation of these nano-object. Based on quantum and *ab initio* calculation, we present a model explaining both the observed two- and four-fold symmetries, for VV and VH configuration, respectively, as well as the changes in G mode.

2 Experimental setup The samples were fabricated by means of standard fabrication techniques [10]. Carbon nanotubes grown by chemical vapour deposition were dispersed from a solution on a SiO_2/Si surface. Prior to the CNT deposition, arrays of metal markers were fabricated on the surface using electron beam lithography technique. Atomic force microscope was used to locate the individual CNTs on the surface with respect to the markers. In Raman experiment the 500 nm^2 metal markers as well as AFM images are used to locate particular nanotube.

All presented Raman spectra were obtained by excitation with a Kr laser (647.14 nm, 1.92 eV, and 676 nm, 1.83 eV) and collected at room temperature using Raman spectrometer (Dilor XY-800) equipped with a charge-coupled device. With a 100× objective lens, the incident laser beam spot has a diameter of ~1 μm, resulting in a power density of ~10^5 W/cm^2 in the Raman active area. Typical resolution is ~1 cm^{-1} and the standard accumulation time is 2×60 seconds. Before measurements the experimental setup was calibrated using CCl_4 and silicon substrates oriented along (100) and (111) crystal axis [11].

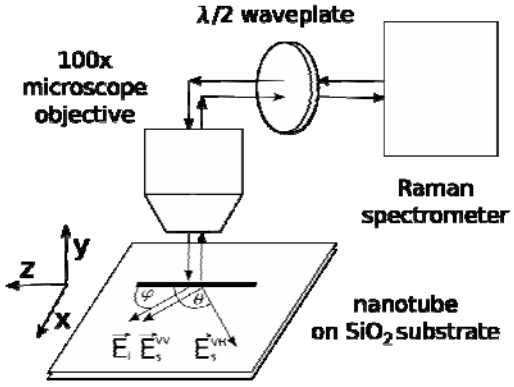

Figure 1 The electric vector $\boldsymbol{E}_{i(s)}$ of the light incident (scattered) from the *Y* direction forms an angle φ ($\theta=\varphi$ for VV or $\theta=\varphi+\pi/2$ for VH configuration) with the nanotube axis, oriented along the *Z* direction. In particular, VH configuration with $\varphi=0$ is denoted as Y(XZ)Y or in the simplified notation (XZ). A half-wave (λ/2) retardation plate is used to change the angle φ.

3 Results Raman spectra of SWNT in the spectral range from 50 cm^{-1} to 3000 cm^{-1} is presented in Fig. 2. Several bands were recorded and identified (RBM, oTO, IFM, D, G, M and G'). Afterwards, using λ/2 waveplate, to change the angle φ, the polarization properties of all bands were studied. Intensity angular dependence follow the $I(\varphi) \propto \cos^4(\varphi)$ and $\cos^2(\varphi)\sin^2(\varphi)$ relation for VV (Fig. 3a) and VH (Fig. 3b) configuration, respectively.

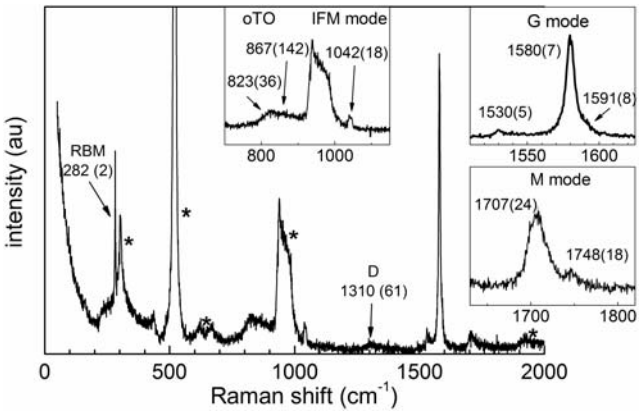

Figure 2 Measured Raman spectrum from individual semiconducting SWNT. Seven bands are observed: RBM, two intermediate frequency, D, G, M and G'. The peak wave numbers are shown together with full width half maxima (FWHM) of various features taken in parentheses. Asterix indicates Si-substrate peaks.

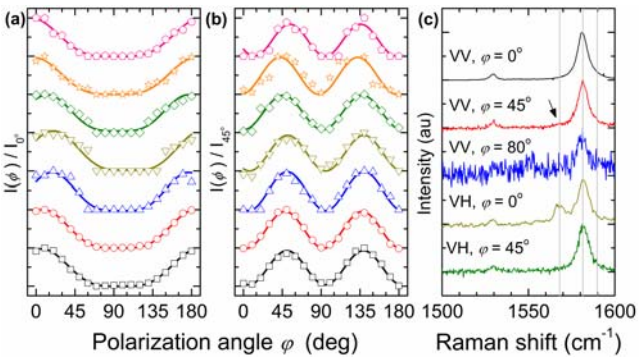

Figure 3 (Color online) Normalized intensity $I(\varphi)/I(0)$ angular φ dependence (see Fig. 1) of seven selected Raman modes (from bottom to top: RBM, G, G', D, M, 823 + 867 cm^{-1}, 1042 cm^{-1}) from one light spot on the isolated semiconducting SWNT sample in two configurations: VV (a) and VH (b). The continuous lines show a fit of data points with the functions $\cos^4(\varphi)$ (a) and $\cos^2(\varphi)\sin^2(\varphi)$ (b). (c) Raman spectra for selected configurations.

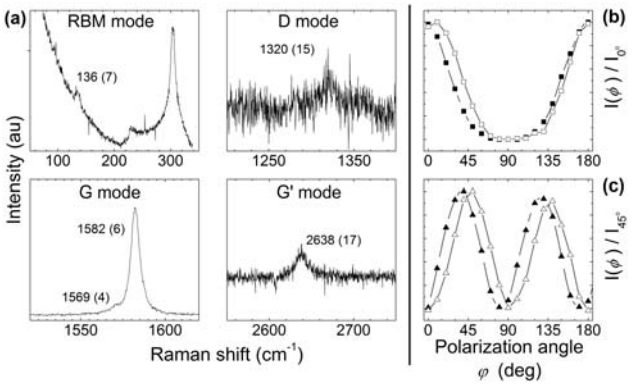

Figure 4 a) Experimental Raman spectrum from one light spot on individual DWNT sample for laser excitation energy EL = 1.92 eV. Four bands are observed: RBM, D, G and G'. The peak wave numbers are shown (with FWHM in parentheses); normalized intensity $I(\varphi)/I(0)$ angular φ dependence of G mode of SWNT (open symbols) and DWNT (full symbols) in two configurations: VV (b) and VH (c).

Significant increase of acquisition time was needed to get visible signals for Y(XX)Y and Y(XY)Y configurations (see Fig. 1). Some quantitative changes in G bands were observed, *e.g.*, for VV $\varphi = 45^o$ and VH $\varphi = 0^o$ configurations the E_{1g} symmetry mode was observed (Fig. 3c).

Similar measurements in the same spectral range have been performed for individual DWNT. Four observed bands (RBM, D, G and G') are presented in Fig. 4a. The intensity angular dependence follows the same relation as in the case of single-wall nanotube (Fig. 4b).

4 Theory One of the simplest descriptions of incident and scattered light polarization influence on Raman scattering efficiency dS is the one with Raman tensor

$$dS \propto \left| \boldsymbol{e}_s \cdot \boldsymbol{R} \cdot \boldsymbol{e}_i \right|^2 ,$$

where $\mathbf{e}_s$, $\mathbf{e}_i$ are scattered and incident light polarization and $\mathbf{R}$ is Raman tensor reflecting the scattering phonon symmetry. For the D_q and the D_{qh} ($q > 3$) point groups and used configuration ($\mathbf{Y}$ direction is neglected) the form of $\mathbf{R}$ is presented in Table 1.

Table 1 Raman tensor for particular phonons' symmetries [12].

$\mathbf{A_{1g}}$	$\mathbf{E_{1g}}$	$\mathbf{E_{2g}}$
$\begin{pmatrix} a & 0 \\ 0 & b \end{pmatrix}$	$\begin{pmatrix} 0 & -d \\ -e & 0 \end{pmatrix}$	$\begin{pmatrix} f & 0 \\ 0 & 0 \end{pmatrix}$

In order to understand the form of Raman tensor, one needs to consider the following issues [8]: 1) light parallel to the nanotube's axis can cause electronic transition in which the symmetry of the electronic wave function does not change ($E_\mu \rightarrow E_\mu$), 2) light perpendicular can cause transition in which the symmetry of the wave function is changed ($E_\mu \rightarrow E_{\mu\pm1}$), 3) the symmetry of the electronic wave function after scattering on the A phonon is the same, 4) is changed ($E_\mu \rightarrow E_{\mu\pm1}$) after scattering on the E_{1g} phonon, 5) is changed ($E_\mu \rightarrow E_{\mu\pm2}$) after scattering on the E_{2g} phonon. Next question is what are the relations between a, b, d, e and f coefficients? In order to study this issue we used the quantum-mechanical description for the Raman scattering process and calculated the electronic and optical properties of SWNT using SIESTA code [13, 14].

The amplitude of Raman scattering (A) described by the third order perturbation theory and in dipole approximation reads as follows

$$A(\omega_i,\omega_s) = \frac{< gv' | \boldsymbol{e}_s \cdot \boldsymbol{p} | e_2v' >< e_2v' | \boldsymbol{H}_{e-p} | e_1v >< e_1v | \boldsymbol{e}_i \cdot \boldsymbol{p} | gv >}{(E_{e_2v'} - E_{gv'} - \hbar\omega_s - i\gamma)(E_{e_1v} - E_{gv} - \hbar\omega_i - i\gamma)},$$

where ω_i, ω_s are incident and scattered photon frequency, g e_1,e_2 are ground and two excited electronic states; v, v' stand for ground and excited phonon states; $\mathbf{p}$ is electron momentum and $\mathbf{H}_{e\text{-}p}$ means electron-phonon interaction matrix. Now we can write the $\mathbf{R}$ tensor in the following form

$$R_{\eta\eta'} \propto \sum_{g,e_1,e_2} \frac{< gv' | \boldsymbol{p}_{\eta'} | e_2v' >< e_2v' | \boldsymbol{H}_{e-p} | e_1v >< e_1v | \boldsymbol{p}_{\eta} | gv >}{(E_{e_2v'} - E_{gv'} - \hbar\omega_s - i\gamma)(E_{e_1v} - E_{gv} - \hbar\omega_i - i\gamma)},$$

where η,η' are x, y or z. The first and third term depends only on the electronic properties of carbon nanotubes and their energy dependence is similar to the imaginary part of the dielectric function ε_2

$$\varepsilon_2(\omega) \propto \mathrm{Im}\left\{ \sum_{g,e} \frac{|< e | \boldsymbol{p} | g >|^2}{E_g - E_e - \hbar\omega - i\gamma} \right\}.$$

The above term includes the selection rules for optical transitions and joint electronic density of states. Comparing ε_2 with the Raman tensor coefficients we get

$$|b|^2 \propto \varepsilon_{\|}^{\,2} \quad , \quad |c|^2, |d|^2 \propto \varepsilon_{\|}\varepsilon_{\perp} \quad , \quad |a|^2, |f|^2 \propto \varepsilon_{\perp}^{\,2} .$$

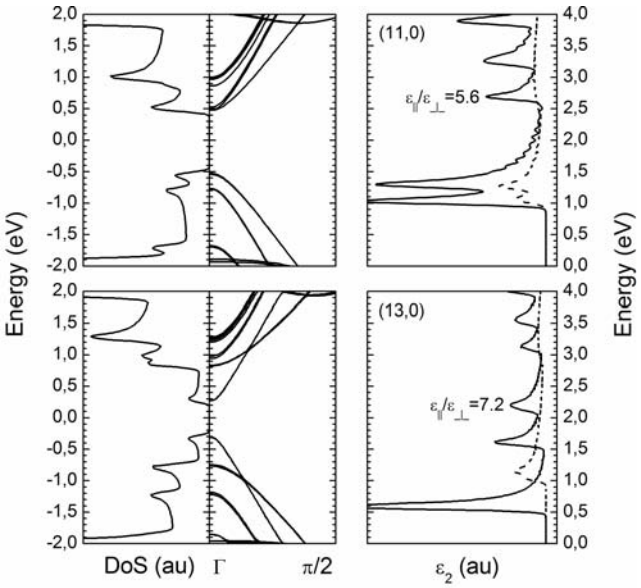

Figure 5 Density of states, band structure and dielectric function of selected semiconducting single-wall carbon nanotubes. Dotted line denotes ε_2 perpendicular to the nanotube axis and solid line denotes ε_2 parallel to the nanotube axis.

Last problem to solve is the shape of the dielectric function $\varepsilon_2(\omega)$. We studied it using SIESTA for a few semiconducting SWNT with diameter around 1nm. For calculations we used standard values of parameters as described in Ref. [15]. Obtained results for nanotubes (11,0) and (13,0) are depicted in Fig. 5.

Here is the interpretation. First, $(I_{ZZ}/I_{XX})_{A1g}$ ratio (connected with the dipolar antenna effect) depends on squared $\varepsilon_\parallel/\varepsilon_\perp$ ratio, which is energy dependent. Theoretically it is possible to obtain $I_{ZZ} < I_{XX}$ for, *e.g.*, E_{12} transition. Second, in the visible energy range there is only one kind of possible optical transition: $E_\mu \rightarrow E_\mu$ (the real electronic transition and the resonant enhancement is the condition under which we are able to observe one particular isolated nanotube). For presented nanotubes the Raman intensity in (XX) configuration is 30-50 times smaller than in (ZZ) even without local depolarization field correction. Moreover, the intensities follow $I_{A1g} > I_{E1g} > I_{E2g}$ due to $\varepsilon_\parallel/\varepsilon_\perp$ ratio (favoured A_{1g} symmetry modes). Third, the band existence has influence on the symmetry of observed phonons. For example, in pure E_{11} transition ($E_\mu \rightarrow E_\mu$, no $E_{\mu\pm1,\,\mu\pm2}$ bands) in the (13,0) nanotube the most intense phonons are the A_{1g} ones. The others are not resonantly enhanced due to lack of final states in the particular energy range. On the other hand, *e.g.* for the E_{11} transition in (11,0) nanotube there are three conduction bands in small energy area and thus observation of phonons with any symmetry is possible due to resonant enhancement.

5 Summary We have presented detailed study of the light polarization influence on the resonant Raman spectra from individual fully spatially isolated single- and double-wall carbon nanotubes. The calculated *ab initio* electronic band structure and imaginary part of the dielectric function, substituted into the standard formula for Raman tensor, well explain observed directional and intensity behaviour of measured spectra as interplay between selection rules and band structure details.

Acknowledgements This work was partly supported by the Polish Council for Science through the Development Grant for the years 2008-2011.

References

[1] G. S. Duesberg, I. Loa, M. Burghard, K. Syassen, and S. Roth, Phys. Rev. Lett. **85**, 5436 (2000).
[2] R. Saito, T. Takeya, T. Kimura, G. Dresselhaus, and M. S. Dresselhaus, Phys. Rev. B **57**, 4145 (1998).
[3] A. Rahmani, J.-L. Sauvajol, S. Rols, and C. Benoit, Phys. Rev. B **66**, 2002 (2002).
[4] A. M. Rao, A. Jorio, M. A. Pimenta, M. S. S. Dantas, R. Saito, G. Dresselhaus, and M. S. Dresselhaus, Phys. Rev. Lett. **84**, 1820 (2000).
[5] A. Jorio, G. Dresselhaus, M. S. Dresselhaus, M. Souza, M. S. S. Dantas, M. A. Pimenta, A. M. Rao, R. Saito, C. Liu, and H. M. Cheng, Phys. Rev. Lett. **85**, 2617 (2000).
[6] A. Jorio, A.G. Souza Filho, V. W. Brar, A.K. Swan, M. S. Unlu, B. B. Goldberg, A. Righi, J.H. Hafner, C.M. Lieber, R. Saito et al., Phys. Rev. B **65**, 121402 (2002).
[7] A. Jorio, M. A. Pimenta, A. G. Souza Filho, Ge. G. Samsonidze, A. K. Swan, M. S. Unlu, B. B. Goldberg, R. Saito, G. Dresselhaus, and M. S. Dresselhaus, Phys. Rev. Lett. **90**, 107403 (2003).
[8] A. Jorio, M. A. Pimenta, C. Fantini, M. Souza, A.G. Souza Filho, Ge. G. Samsonidze, G. Dresselhaus, M. S. Dresselhaus, and R. Saito, Carbon **42**, 1067 (2004).
[9] E. B. Barros, A. Jorio, Ge. G. Samsonidze, R. B. Capaz, A. G. Suoza Filho, J. M. Filho, G. Dresselhaus, and M. S. Dresselhaus, Phys. Rep. **431**, 261 (2006).
[10] M. Zdrojek, T. Melin, W. Gebicki, H. Desienger, D. Stievenard, and L. Adamowicz, J. Appl. Phys. **100**, 114326 (2006).
[11] K. Mizoguchi and S. Nakashima, J. Appl. Phys. **65**, 2583 (1988).
[12] Cardona and G. Guntherodt (Ed.), Light Scattering in Solids II, Topics in Applied Physics, Vol. 50 (Springer, Berlin, 1982).
[13] J. M. Soler, E. Artacho, J. D. Gale, A. Garcia, J. Junquera, P. Ordejon, and D. Sanchez-Portal, J. Phys.: Condens. Matter **14**, 2745 (2002).
[14] D. Sanchez-Portal, E. Artacho, J. M. Soler, A. Rubio, and P. Ordejon, Phys. Rev. B **59**, 12678 (1999).
[15] K. V. Christ and H. R. Sadeghpour, Phys, Rev. B **75**, 195418 (2007).